

TERRIGENOUS MATERIAL SUPPLY TO THE PERUVIAN CENTRAL CONTINENTAL  
SHELF (PISCO 14°S) DURING THE LAST 1000 yr: PALEOCLIMATIC IMPLICATIONS.

F. Briceño-Zuluaga<sup>1,2</sup>, A. Sifeddine<sup>1,2,3</sup>, S. Caquineau<sup>2,3</sup>, J. Cardich<sup>1,2</sup>, R. Salvattecí<sup>5</sup>, D.  
Gutierrez<sup>2,4</sup>, L. Ortlieb<sup>2,3</sup>, F. Velazco<sup>2,4</sup>, H. Boucher<sup>2,3</sup>, C. Machado<sup>1,2</sup>.

<sup>1</sup> Departamento de Geoquímica, Universidade Federal Fluminense - UFF, Niterói, RJ – Brasil.

<sup>2</sup> LMI PALEOTRACES (IRD-France, UPMC-France, UA-Chile, UFF-Brazil, UPCH-Peru).

<sup>3</sup> IRD-Sorbonne Universités (UPMC, CNRS-MNHN), LOCEAN, IRD France-Nord, Bondy,  
France.

<sup>4</sup> Instituto del Mar del Peru IMARPE. Esquina Gamarra y General Valle s/n, Callao 22000, Peru

<sup>5</sup> Institute of Geoscience, Kiel University, Germany.

Correspondence to: franciscojavier@id.uff.br

**Abstract**

In the Eastern Pacific, lithogenic input to the ocean responds to variations of the atmospheric and oceanic system and their teleconnections over different timescales. Atmospheric (e.g., wind fields), hydrological (e.g., fresh water plumes) and oceanic (e.g., currents) conditions determine the transport mode and the amount of lithogenic material transported from the continent to the continental shelf. Here, we present the grain size distribution of a composite record of two laminated sediment cores retrieved from the Peruvian continental shelf that record the last ~1000 yr at a sub-decadal to centennial time-series resolution. We propose novel grain-size indicators of wind intensity and fluvial input that allow reconstructing the oceanic-atmospheric variability modulated by sub-decadal to centennial changes in climatic conditions. Four grain size modes were identified. Two are linked to aeolian inputs (M3: ~54  $\mu\text{m}$  and M4: ~91  $\mu\text{m}$  on average), the third is interpreted as a marker of sediment discharge (M2: ~10  $\mu\text{m}$  on average), and the last is without an associated origin (M1: ~3  $\mu\text{m}$ ). The coarsest components (M3 and M4) dominated during the Medieval Climate Anomaly (MCA) and the Current Warm Period (CWP) periods, suggesting that aeolian transport increased as consequence of surface wind stress intensification. In contrast, M2 displays an opposite behavior, exhibiting an increase in fluvial terrigenous input during the Little Ice Age (LIA) in response to more humid conditions associated with El Niño like conditions. Comparison with other South American paleoclimate records indicates that the observed changes are driven by interactions between meridional displacement of the Intertropical Convergence Zone (ITCZ), the South Pacific Sub-tropical High (SPSH) and Walker Circulation at decadal and centennial time scales.

The Pisco region (~14-15°S) hosts one of the most intense coastal upwelling cells off Peru due to the magnitude and persistence of alongshore equatorward winds during the annual cycle (Fig. 1B). Regional winds can also be affected at interannual timescales by El Niño Southern Oscillation (ENSO) variability (i.e., enhanced or weakened during La Niña and El Niño events, respectively), as well as by the Pacific Decadal Oscillation (PDO) at decadal timescales (Flores-Aqueveque et al., 2015). These factors also affect the inputs of terrigenous material to the Peruvian continental shelf. Saukel et al. (2011) found that wind is the major transport agent of terrigenous material west of the Peru–Chile Trench between 5°S and 25°S. Flores-Aqueveque et al. (2012) showed that in the arid region of northern Chile, transport of aeolian coarser particles (approximately ~100 µm) is directly related to interannual variations in the domain of the strongest winds. The Pisco region is also home to local dust storms called “Paracas”, which transport dust material to the continental shelf as a response to seasonal erosion and transport events in the Ica desert (~15°S). This process reflects atmospheric stability conditions and coastal sea surface temperature connections (Gay, 2005). In contrast, sediment fluvial discharge is more important on the northern coast of Peru where there are large rivers, and it decreases southward where arid conditions are dominant (Garreaud and Falvey, 2009; Scheidegger and Krissek, 1982). This discharged material is redistributed southward by coastal currents along the continental shelf (Montes et al., 2010; Smith, 1983). In addition, small rivers exist in our study area, such as the Pisco River, which can increase their flow during strong El Niño events (Bekaddour et al., 2014). It has also been demonstrated that during El Niño events and coincident positive PDO, there is an increase in precipitation along northern Peru and, consequently, higher river discharge, mainly from the large rivers (e.g., the Santa River), whereas an opposite behavior is observed during La Niña events and negative phase of PDO (Bekaddour et al., 2014; Böning and Brumsack, 2004; Lavado Casimiro et al., 2012; Ortlieb, 2000; Rein, 2005, 2007; Scheidegger and Krissek, 1982; Sears, 1954).

Grain size distributions in marine sediments may indicate different sources and/or depositional processes that can be expressed as polymodal distributions (e.g., Pichevin et al., 2005; Saukel et al., 2011; Stuut and Lamy, 2004; Stuut et al., 2002, 2007; Sun et al., 2002; Weltje and Prins, 2003, 2007). The polymodal distribution makes the classification of grain size composition an essential step in identifying the different sedimentary processes and the past environmental conditions behind them (e.g., climate, atmosphere and ocean circulation) (Bloemsma et al., 2012; Flores-Aqueveque et al., 2012, 2015; Pichevin et al., 2005; Ratmeyer et al., 1999; Saukel et al., 2011; Stuut et al., 2005, 2007; Sun et al., 2002). The grain-size distributions of lithogenic materials in marine sediments can thus be used to infer relative wind strengths and aridity on the assumption

that more vigorous atmospheric circulation will transport coarser particles to a greater distance and that the relative abundance of fluvial particles reflects precipitation patterns (e.g., Hesse and McTainsh, 1999; Parkin and Shackleton, 1973; Pichevin et al., 2005; Stuut and Lamy, 2004; Stuut et al., 2002).

A significant number of studies have described the climatic, hydrologic and oceanographic changes during the last 1000 years on the Peruvian continental shelf (Ehlert et al., 2015; Gutiérrez et al., 2011; Salvattecí et al., 2014b; Sifeddine et al., 2008). Evidences of changes in the Humboldt Current circulation system and in the precipitation pattern have been reported. Salvattecí et al., (2014b) show that the Medieval Climatic Anomaly (MCA) exhibits two distinct patterns of Peruvian upwelling characterized by weak/intense marine productivity and sub-surface oxygenation, respectively, as a response to the intensity of SPSH linked to the Walker circulation. During the Little Ice Age (LIA), an increased sediment discharge over the Pisco continental shelf was described, as well as a stronger oxygenation and lower productivity (Gutiérrez et al., 2009; Salvattecí et al., 2014b; Sifeddine et al., 2008). In addition, during the Current Warm Period (CWP), the PUE exhibited 1) an intense Oxygen Minimum Zone (OMZ) and an increase in marine productivity, 2) a significant SST cooling ( $\sim 0.3\text{--}0.4^{\circ}\text{C decade}^{-1}$ ), and 3) an increase in terrigenous material input (Gutiérrez et al., 2011).

Here we present new data regarding the effective mode of transport of mineral fractions to the Pisco shelf during the last millennium, confirming previous work and bringing new highlights about the climatic mechanism behind Humboldt circulation and atmospheric changes, especially during the MCA. Our results identify wind intensification during second part of the MCA and CWP, in contrast to a decrease of the wind intensity during the LIA and the first part of the MCA synchronous with fluvial discharge increases. Comparisons with other paleoclimate records indicate that the ITCZ displacement, the SPSH and the Walker circulation were the main drivers for the hydroclimate changes along the coastal Peruvian shelf during the last millennium.

## **2. Sedimentary settings.**

Reinhardt et al., (2002); Suess et al., (1987) and Gutierrez et al., (2006) described the sedimentary facies in the Peruvian shelf and the role of currents in the erosion process as well as the redistribution and favorable hemipelagic sedimentation of material over the continental shelf. These studies showed that high resolution sediment records are present in specific localities of the Peruvian continental margin. Suess et al., (1987) described the two sedimentary characteristic facies between  $6 - 10^{\circ}\text{S}$  and between  $11 - 16^{\circ}\text{S}$ . The first one,  $6 - 10^{\circ}\text{S}$  (Salaverry Basin), is characterized by no hemipelagic sediment accumulation because in this zone the southward poleward undercurrent is strong. The second one,  $11 - 16^{\circ}\text{S}$  Lima Basin, is characterized by a lens shaped depositional center of organic-rich mud facies favored by oceanographic dynamics

from the position and low velocity of the southward poleward current on the continental shelf (Reinhardt et al., 2002; Suess et al., 1987). High-resolution sediment echo sounder profiles further characterize the mud lens nature and complement the continental shelf information (Salvatteci et al., 2014a). These upper mud lenses are characterized by fine grain size, a diatomaceous, hemiplegic mud with high organic carbon, and the absence of erosive and bioturbation process.

The Pisco continental shelf sediments are a composite of laminated structures characterized by an array of more or less dense sections of dark and light millimetric bands (Brodie and Kemp, 1994; Salvatteci et al., 2014a; Sifeddine et al., 2008). The laminae structure and composition result from a complex interplay of factors including the terrigenous material input (both aeolian and fluvial), the upwelling productivity, and associated particle export to the seafloor (Brodie and Kemp, 1994; Salvatteci et al., 2014a). The anoxic conditions favored by an intense OMZ (Gutiérrez et al., 2006) and weak current activity at some areas (Reinhardt et al., 2002; Suess et al., 1987) encourage the preservation of paleo-environmental signals and consequently a successful recording of the environmental and climate variability.

Along the Peruvian coast, lithogenic fluvial material is supplied by a series of large rivers that are more significant to the north of the study area (Lavado Casimiro et al., 2012; McPhillips et al., 2013; Morera et al., 2011; Rein, 2005; Scheidegger and Krissek, 1982; Unkel et al., 2007). In fact, Smith, (1983) concluded that sedimentary material can be transported for long distances in an opposite direction of prevailing winds and surface currents in upwelling zones. In fact, the coastal circulation off Peru is dominated by the poleward Peru-Chile undercurrent (PCUC), which flows over the outer continental shelf and upper continental slope, whereas the equatorward Peru coastal current is limited to a few dozens of meters in the surface layer (Chaigneau et al., 2013). On the other hand, several works have shown that precipitation, fluvial input discharge (Bekaddour et al., 2014; Bendix et al., 2002; Lavado-Casimiro and Espinoza, 2014), and the PCUC increase during the El Niño events (Hill et al., 1998; Strub et al., 1998; Suess et al., 1987). These observations suggest a potential for the fluvial particles to spread over the continental margin under wet paleoclimatic conditions (e.g., El Niño or El Niño-like). Lithogenic material in the study area might also originate from wind-driven dust storms or “Vientos Paracas”, which are more frequent and intense during Austral winters (Escobar Baccaro, 1993; Gay, 2005; Haney and Grolier, 1991) and by the saltation and suspension mechanisms with which this material reaches the continental shelf.

### **3. Materials and Methods**

#### **3.1. Stacked record.**

The B040506 “B06” (14° 07.90’ S, 76° 30.10’ W, 299 m water depth) and the G10-GC-01 “G10” (14° 22.96’ S, 076° 23.89’ W, 313 m water depth) sediment cores were retrieved from the central Peruvian continental shelf in 2004 during the Paleo2 cruise onboard the Peruvian José Olaya Balandra vessel (IMARPE) and in 2007 during the Galathea-3 cruise, respectively (Fig. 1A). We compared the age models and performed a laminae cross-correlation between the two cores in order to develop a continuous record for the last millennium (Salvatteci et al., 2014a) (Fig. 1S). The choice of these two cores was based on previous detailed stratigraphic investigations and available complementary multi-proxy reconstructions (Gutiérrez et al., 2006, 2009; Salvatteci et al., 2012, 2014a, 2014b; Sifeddine et al., 2008). The boxcore B06 (0.75 m length) is a laminated core with a visible slump at ~52cm and 3 thick homogeneous deposits (1.5 to 5.0 cm thick) identified in the SCOPIX images. These intervals were not considered in our study (Fig. 1S). The presence of filaments of the giant sulphur bacteria *Thioploca* spp in the top of core B06 confirms the successful recovery of the sediment water interface.

According to the biogeochemical analysis in Gutierrez et al., (2009) (i.e., Palynofacies, Oxygen Index (Rock-Eval), total organic carbon and  $\delta^{13}\text{C}$ ), B06 is characterized by a distinctive shift at ~30 cm. More details are provided by Sifeddine, et al. (2008), Gutiérrez et al. (2009) and Salvatteci et al., (2014a). The age model of B06 was inferred from five  $^{14}\text{C}$ -calibrated AMS age distributions (Fig. 1S), showing that this core covers the last ~700 yr. For the last century, which is recorded only by B06, the age model was based on downcore natural excess  $^{210}\text{Pb}$  and  $^{137}\text{Cs}$  distributions and supported by bomb-derived  $^{241}\text{Am}$  distributions (Fig. 2S and Gutiérrez et al., (2009). The mass accumulation rate after ca. 1950AD was  $0.036 \pm 0.001 \text{ g cm}^{-2} \text{ y}^{-1}$  and before ca. 1820AD was  $0.022 \pm 0.001 \text{ g cm}^{-2} \text{ y}^{-1}$ . On the other hand, the G10 is a gravity laminated sediment core of 5.22 m presenting six units and exhibiting some minor slumping. The G10 age model was based on thirty one samples of  $^{14}\text{C}$ -calibrated AMS age distributions, showing that the core covers the Holocene period (Salvatteci et al., 2014b, 2016). Here we used only a laminated section between ~18 - 45 cm that chronologically covered part of the MCA period (from ~1050 to 1500) and presented no slumps (Fig. 1S).

The spatial regularity of the initial core sampling combined with the naturally variable sedimentation rate implied variable time rates between samples (150 samples in total). Each sample is 0.5 cm thick in B06 and usually includes 1-2 laminae. On the other hand in core G10: each sample is 1 cm thick including 3-4 laminae. The results considering the sedimentation rates showed that the intervals during MCA, LIA and CWP span between 18, 7, and 3 years, respectively. Because of differences in the subsampling thickness between cores and variable sedimentation rates, results are binned by 20 year intervals (the lowest time resolution among samples) after linear interpolation and 20-yr running mean of the original data set.

### 3.2. Grain size analyses

To isolate the mineral terrigenous fraction, organic matter, calcium carbonate and biogenic silica were successively removed from approximately 100 mg of bulk sediment sample using H<sub>2</sub>O<sub>2</sub> (30% at 50°C for 3 to 4 days), HCl (10% for 12 hours) and Na<sub>2</sub>CO<sub>3</sub> (1 M at 90°C for 3 hours) respectively. Between each chemical treatment, samples were repeatedly rinsed with deionized water and centrifuged at 4000 rpm until neutral pH. After pre-treatment, the grain size distribution was determined with an automated image analysis system (model FPIA3000, Malvern Instruments). This system is based on a CCD (Charge Coupled Device) camera that captures images of all of the particles homogeneously suspended in a dispersal solution by rotation (600 rpm) in a measurement cell. After magnification ( $\times 10$ ), particle images are digitally processed and the equivalent spherical diameter (defined as the diameter of the spherical particle having the same surface as the measured particle) is determined. The optical magnification used ( $\times 10$ ) allows the counting of particles with equivalent diameters between 0.5 and 200  $\mu\text{m}$ . Prior to the FPIA analysis, all samples were sieved with a 200- $\mu\text{m}$  mesh in order to recover coarser particles. Since particles  $> 200 \mu\text{m}$  were never found in any samples, the grain size distribution obtained by the FPIA method reliably represents the full particle size range in the sediment. A statistically significant number of particles (hundreds of thousands up to 300,000) are automatically analyzed by FPIA, providing particle size information comparable to that obtained with a laser granulometer along with images of the individual particles. Using the images to check the efficiency of the pre-treatments, we ensured that both organic matter and biogenic silica had been completely removed from all the samples. Finally, particle countings were binned into 45 different size bins between 0.5 and 200 micron instead of the 225 set by the FPIA manufacturer in order to reduce errors related to the presence of very few particles in some of the preselected narrow bins. Grain size distributions are expressed as (%) volume distributions.

### 3.3. Determining sedimentary components and the de-convolution fitting model

As different particle transport/deposition processes are known to influence the grain-size distribution of the lithic fraction of sediment (e.g. Holz et al., 2007; Pichevin et al., 2005; Prins et al., 2007; Stuut et al., 2005, 2002; Sun et al., 2002; Weltje and Prins, 2003, 2007; Weltje, 1997), identifying the individual components of the polymodal grain size distribution is decisive for paleoenvironmental reconstructions. The numerical characteristics [i.e., amplitude A, geometric mean diameter (Gmd), and geometric standard deviation (Gsd) of the individual grain size populations whose combination forms the overall grain size distribution] were determined for all samples using the iterative least-square method of Gomes et al. (1990). This fitting method aims to minimize the squared difference between the measured volume-grain size distribution and the one computed from a mathematical expression based on log-normal function. The number of

individual grain size populations to be used is determined by the operator, and all statistical parameters (A, Gmd and Gsd) are allowed to change from one sample to another. This process presents a strong advantage compared to end-member modeling (e.g., Weltje 1997) in which the individual grain size distributions are maintained constant over the whole time series, the only fitting parameter being the relative amplitude, A. Indeed, it is unlikely that the parameters that govern both transport and deposition of lithogenic material, and therefore grain size of particles, remain constant over time. In turn, variations of these parameters are expected to induce change of the grain size distribution parameters such as Gmd and Gsd.

## **4. Results and discussion**

### **4.1. Basis for interpretation**

Both sediment cores (B06 and G10) exhibit roughly bimodal grain-size distribution presenting significant variation in amplitude and width. These modes correspond to fine-grain-size classes from ~3 to 15  $\mu\text{m}$  and coarser grain size classes between ~50 and 120  $\mu\text{m}$  (Fig. 3S). A principal component analysis (PCA) based on the Wentworth (1922) grain-size classification identifies four modes that could explain the total variance of the dataset (Fig. 4S). The measured and computed grain size distributions show high correlations ranging from  $R^2=0.75$  to 0.90, attesting that using 4 grain size modes is well adapted to our sediment samples and that the computed ones may be reliable for further interpretation (Fig. 2). Lower correlations only occurred for 6 samples that are characterized by small proportions of terrigenous material compared to biogenic silica, organic matter and carbonates. In these cases, the number of lithic particles remaining after chemical treatments was small, which increased the associated relative error. However, these samples have been included in the data set since they all presented a high contribution of coarser particles.

Grain size parameters are presented in Table 1. The first mode (M1), with a Gmd of approximately  $3 \pm 1 \mu\text{m}$ , and the second one (M2), with a Gmd of  $10 \pm 2 \mu\text{m}$ , are characterized by large Gsd ( $\sim 2\sigma$ ), indicating a low degree of sorting. Such low degree of sorting suggests a slow and continuous depositional process as occurs in other environments (Sun et al., 2002). The coarsest modes M3 and M4 display mean Gmd values of  $54 \pm 12 \mu\text{m}$  and  $91 \pm 13 \mu\text{m}$ , respectively. These modes present Gsd values close to  $1\sigma$ . The Gmd values of the two coarsest modes are consistent with the optimal grain size transported under conditions favorable to soil erosion (lack of vegetation, low threshold friction velocity, surface roughness and low soil moisture) and low wind friction velocity (Iversen and White, 1982; Kok et al., 2012; Marticorena and Bergametti, 1995; Marticorena, 2014; Shao and Lu, 2000). Such conditions prevail in the studied area because the central coastal Peru consists of a sand desert area characterized by no rain, a lack of vegetation and persistent wind (Gay, 2005; Haney and Grolier, 1991).

In the vicinity of desert areas, where wind-blown transport prevails, particles with grain size as high as  $\sim 100\ \mu\text{m}$  can accumulate in marine sediments (e.g., Flores-Aqueveque et al., 2015; Stuut et al., 2007) or even in lacustrine sediments (An et al., 2012). Indeed, Stuut et al., (2007) reported the presence of distributions typical of wind-blown particles with  $\sim 80\ \mu\text{m}$  grain size ( $\sim 29^\circ\text{S}$  North Chile) that is consistent with our results. In the studied area, the emission and the transport of mineral particles are related to the strong wind events called “Paracas”. Paracas dust emission is a local seasonal phenomenon that preferentially occurs in winter (July-September) and is due to an intensification of the local surface winds (Escobar Baccaro, 1993; Haney and Grolier, 1991; Schweigger, 1984). The pressure gradient of sea level between  $15^\circ\text{--}20^\circ\text{S}$ ,  $75^\circ\text{W}$  is the controlling factor of Paracas winds (Quijano, 2013), along with local topography (Gay, 2005). Coarse particles found in continental sediments off Pisco cannot have a fluvial origin because substantial hydrodynamic energy is necessary to mobilize particles of this size ( $50\text{--}100\ \mu\text{m}$ ), and this region is devoid of large rivers (Reinhardt et al., 2002; Scheidegger and Krissek, 1982; Suess et al., 1987).

Therefore, the coarsest modes (M3 and M4) can be interpreted as markers of aeolian transport resulting from surface winds and emission processes (Flores-Aqueveque et al., 2015; Hesse and McTainsh, 1999; Marticorena and Bergametti, 1995; McTainsh et al., 1997; Sun et al., 2002) and indicate a local and proximal aeolian source (i.e., Paracas winds). This interpretation is in contrast to the Atacama Desert source suggested by Ehlert et al., (2015) and Molina-Cruz, (1977). Ehlert et al. (2015), who used the same sediment core (B06), and also indicated difficulties in the interpretation of the detrital Sr isotopic signatures as an indicator of the terrigenous sources. These difficulties can be associated with the variability of the  $^{87}\text{Sr}/^{86}\text{Sr}$  due to grain size (Meyer et al., 2011). The finest M1 component ( $\sim 3\ \mu\text{m}$ ) may be linked to both aeolian and fluvial transport mechanisms. Thus, because its origin is difficult to determine, and because its trend appears as relatively independent from the other components, we do not further use it.

The M2 component ( $\sim 10\ \mu\text{m}$ ) is interpreted as an indicator of fluvial transport (Koopmann, 1981; McCave et al., 1995; Stuut and Lamy, 2004; Stuut et al., 2002, 2007). Indeed, this is consistent with the report by Stuut et al., (2007) for the fluvial mud ( $\sim 8\ \mu\text{m}$ ) in the South of Chile ( $>37^\circ\text{S}$ ) where the terrigenous input is dominated by fluvial origins. A fluvial origin of this M2 component is also supported by showing the same trend in the geochemical proxies, such as radiogenic isotope compositions of detrital components (Ehlert et al., 2015), mineral fluxes (Sifeddine et al., 2008) or %Ti (Salvatteci et al., 2014b), indicating more terrigenous transport during the LIA, when humid conditions were dominant. The M2 component is interpreted as being linked to river material discharge, mostly from the north Peruvian coast, and redistribution by the PCUC and bottom currents (Montes et al., 2010; Rein et al., 2004; Scheidegger and Krissek, 1982; Unkel et al., 2007).



## 4.2. Aeolian and fluvial input variability during the past ~1000 yr

Grain size component (M2, M3 and M4; Table 1) variations in the composite records (B06 and G10) express changes in wind stress and fluvial runoff at multi-decadal to centennial scales during the last millennium. The sediments deposited during the MCA exhibit two contrasting patterns of grain size distributions. A first sequence dated from 1050 to 1170 AD has, low values of  $D_{50}$  (i.e., median grain size) that vary around  $16 \pm 6 \mu\text{m}$  and are explained by  $50 \pm 14\%$  M2,  $16 \pm 8\%$  M3,  $21 \pm 5\%$  M4 and  $13 \pm 5\%$  M1 contributions. A second sequence, dated from 1170 to 1450 AD, was marked by high values of  $D_{50}$  in the range of  $34 \pm 18 \mu\text{m}$ , with average contributions of  $36 \pm 8\%$  for M2,  $21 \pm 10\%$  for M3,  $29 \pm 15\%$  for M4 and  $14 \pm 6\%$  for M1. These results indicate high variability of transport of particles during the MCA, with more fluvial sediment discharge from 1050 to 1170, followed by an aeolian transport increase between 1170 and 1450 AD (Fig. 3).

During the LIA (1450 – 1800 AD), the deposited particles were dominated by fine grain sizes with a  $D_{50}$  varying around an average of  $15 \mu\text{m}$ , explained by  $53 \pm 15\%$  M2 contribution. In contrast, the contribution of M3 averaged  $19 \pm 9\%$  and ranged from 4 to 45%, whereas M4 showed an average contribution of  $14 \pm 11\%$  and varied from 0 to 44% during the same period. The dominant contribution of the finest-sized particles of M2 suggests a high fluvial terrigenous input to the Peruvian continental shelf. It is important to note that M2 contributions increased from the beginning to the end of the LIA at ~1800 AD, suggesting a gradual increase in fluvial sediment discharge input related to the enhancement of the continental precipitation (Fig. 3C). Indeed, during the LIA, our results confirm previous interpretations of wet conditions along the Peruvian coast (Gutiérrez et al., 2009; Salvattecchi et al., 2014b; Sifeddine et al., 2008). These results also imply that this period was characterized by weak surface winds and hence a weaker coastal upwelling.

Subsequently,  $D_{50}$  variations show multidecadal variability during the last ~200 yr that is divided into three distinctive periods. The first one from ~1800 to 1850 AD shows dominance of coarse particles around  $50 \mu\text{m}$ , explained by the high contribution of M3 and M4 (up to 45% and 50% respectively) during this period. These results suggest a period of drier climate and very strong wind conditions. The second one from 1850 to 1900 AD displays values around  $\sim 20 \mu\text{m}$  explained by  $\sim 40\%$  of M2,  $\sim 20\%$  of M3 and  $\sim 20\%$  of M4 that suggests that fluvial sediment discharge was the dominant transport mechanism, although not as significant as during the LIA. The third period spans from 1900 AD to the final part of record and covers the CWP. Our results reveal a dominance of coarse particles during the most of this period ( $D_{50}$  up to of  $80 \mu\text{m}$ ) that arise from high contributions of M3 and M4 ( $\sim 40\%$  and  $\sim 50\%$  respectively). However a clear decrease of the  $D_{50}$  is displayed at the end of this period that is explained by a decrease of contributions of the aeolian component M4 ( $\sim 20\%$ ), although the contribution of M3 and M2 remain relatively

stable (~25% and 30%, respectively). These conditions display no clear dominance of a given transport mode during this time. In addition, markedly coarser particles in the M4 component were very common during this time (the last 200yr), indicating a strong probability of extreme wind stress events (Fig. 3F).

#### 4.3. Climatic interpretations

Our findings suggest a combination of regional and local atmospheric circulation mechanism changes that controlled the pattern of sedimentation in the study region. Our record is located under the contemporary seasonal Paracas dust storm path, but it also records discharged fluvial muds that are supplied by the rivers along the Peruvian coast. Hence, this record is particularly well suited for a reconstruction of continental runoff/wind intensity in the central Peruvian continental shelf during the last millennium. The interpretation of the changes in the single records of the components (M2, M3 and M4) and their associations (e.g., ratios) can reflect paleoclimatic variations in response to changes in atmospheric conditions. Here, we used the ratio between the aeolian components, defined as the contribution of the stronger winds over total wind variability:  $M4/(M3+M4)$ . We consider this ratio as a proxy of the local wind surface intensity and thus as of the SPSH atmospheric circulation (Fig. 4A). Previous studies have similarly and successfully used grain-size fraction ratios as paleoclimate proxies of atmospheric conditions and circulation to explain other sediment records (Holz et al., 2007; Huang et al., 2011; Prins, 1999; Shao et al., 2011; Stuut et al., 2002; Sun et al., 2002; Weltje and Prins, 2003).

As explained above, the MCA was characterized by a sine-like peak structure that depicts two different climate stages. During the first stage spanning from ~1050 to 1170 AD the fluvial input show a peak centered at 1120 AD linked to a precipitation increase accompanied by a decrease in wind intensity. Those results suggest a southward ITCZ displacement (Fig. 4E) as a response to more El Niño like conditions as suggested by Rustic et al., (2015) (Fig 4 G and H). In contrast, during the second stage the surface winds had their greatest intensity with a peak centered at ~1200 AD as a consequence of displacement of the ITCZ-SPSH system. The displacement of the SPSH core towards eastern South American coast intensified alongshore winds as a regional response to stronger Walker circulation. These features are in agreement with the ocean thermostat mechanism proposed by Clement et al., (1996). This mechanism produces a shallow thermocline in the eastern pacific (Fig. 4G and H) and consequently more intense upwelling conditions and a stronger OMZ offshore of Pisco recorded in low values of the Re/Mo ratio (Fig. 4D). These two patterns (i.e., enhanced fluvial transport/enhanced wind intensity) might have been triggered by the expression of Pacific variability at multidecadal timescales with the combined action of the Atlantic Multidecadal Oscillation (AMO). Indeed other works provide evidence during the MCA for low South American Monsoon System (SAMS) activity at

multidecadal timescales driven by the AMO (Fig. 4F) (Apaéstegui et al., 2014; Bird et al., 2011; Reuter et al., 2009). Thus, besides the displacement of the ITCZ', the AMO could have modulated Walker circulation at a multidecadal variability during the MCA through mechanisms such as those described by McGregor et al., (2014) and Timmermann et al., (2007).

Our results, combined with other paleo-reconstructions, suggest that the LIA was accompanied by a weakening of the regional atmospheric circulation and of the upwelling favorable winds. During the LIA, the mean climate state was controlled by a gradual intensification of the fluvial input of sediments to the continental shelf, thus indicating more El Niño-like conditions (Fig. 4B). These features are confirmed by an increase of the terrigenous sediment flux, as described by Sifeddine et al. (2008) (Fig 4C) and Gutierrez et al., (2009) and by changes of the radiogenic isotopic composition of the terrigenous fraction (Ehlert et al., 2015). These wet conditions are also marked by an intensification of the South American Monsoon System (SAMS) and the southern meridional displacement of the ITCZ, as evidence by paleo-precipitation records in the Andes and in the Cariaco Trench (Apaéstegui et al., 2014; Haug et al., 2001; Peterson and Haug, 2006) (Fig. 4E). At the same time, a prevalence of weak surface winds (Fig.4A) and an increase of subsurface oxygenation driving sub-oxic conditions in the surface sediment are recorded (Fig. 4D). These characteristics also support the hypothesis of the ITCZ-SPSH southern meridional displacement and are consistent with a weakening of the Walker circulation (Fig. 4G).

The transition period between the LIA and CWP appears as an abrupt event showing a progressive positive anomaly in the wind intensity synchronous with a rapid decrease in fluvial input to the continental shelf (Fig. 4A and B). This transition suggests a rapid change of meridional (ITCZ-SPSH) and zonal (Walker) circulation interconnection, which controls the input of terrigenous material (Fluvial/Aeolian). Gutiérrez et al. (2009) found evidence of a large reorganization in the tropical Pacific climate with immediate effects on ocean biogeochemical cycling and ecosystem structure at the transition between the LIA and CWP. The increase in the regional wind circulation that favors aeolian erosive processes simultaneously leads to an increase in the OMZ intensity related to upwelling intensification.

Finally, during the CWP (~1900 A.D. to present), a trend to steadying of low fluvial input (Fig. 4B) was combined with an increase in wind intensity (Fig. 4A) that was coupled to a strong OMZ. This setting suggests the northernmost ITCZ-SPSH system position. This hypothesis is supported by other studies on the continental shelf of Peru (Salvatteci et al., 2014b) and also in the Eastern Andes where a decrease in rainfall of between ~10 – 20% relative to the LIA was reported for the last century (Reuter et al., 2009). Enhancement of wind intensity is also consistent with the multidecadal coastal cooling and increase of upwelling productivity since the late nineteenth century (Gutiérrez et al., 2011; Salvatteci et al., 2014b; Sifeddine et al., 2008) and confirms the

relations between the intensification of the upwelling activity induced by the variability of the regional wind intensity from SPSH displacement.

The increase in the wind intensity over the past two centuries likely represents a result of the modern positioning of the ITCZ – SPSH system and the associated intensification of the local and regional winds (Fig. 4A). The contributions of aeolian deposition material (Fig. 3E and F) and in consequence the wind intensity and its variability during the last 100 yr are stronger than during the second sequence of the MCA (Fig. 4A) under similar conditions (i.e., position of the ITCZ-SPSH system). This variability implies a forcing mechanism in addition to the enhancement of the wind intensity, one that may be related to the current climate change conditions (Bakun, 1990; England et al., 2014; Sydeman et al., 2014). Moreover, during the CWP, the wind intensity showed a direct-relation with OMZ strength (Fig. 4A and D) that suggests an increase in the zonal gradient and thus in the Walker circulation on a multidecadal scale.

Our record shows that on a centennial scale, the fluvial input changes are driven by the meridional ITCZ position and a weak gradient of the Walker circulation, consistent with El Niño like conditions. In contrast, variations of the surface wind intensity are linked to the position of the SPSH modulated by both the meridional variation of the ITCZ and the intensification of the zonal gradient temperature related with the Walker circulation and expressing La Niña like conditions. A clear relation between the zonal circulation and wind intensity at a centennial time scale is displayed. All these features modulate the biogeochemical behavior of the Peruvian upwelling system.

## Conclusions

Study of the grain size distribution in laminated sediments from the Pisco Peruvian shelf has allowed the reconstruction of changes in wind intensity and terrigenous fluvial input at centennial and multidecadal time scales during the last millennium. The long-term variation of M2 ( $\sim 10\mu\text{m}$ ) mode is an indicator of hemipelagic fluvial input related to the regional precipitation variability. Meanwhile, the M3 ( $54\pm 11\mu\text{m}$ ) and M4 ( $91\pm 11\mu\text{m}$ ) components are related to aeolian transport and thus with both local and regional wind intensity. The temporal variations of these fractions indicate that the MCA and CWP periods were characterized by an increment in the coarse particle transport (M3 and M4) and thus an enhancement of the surface wind intensity, whereas the LIA was characterized by stronger fluvial input as evidence from an increase of fine (M2) particles. Comparison between records reveals a coherent match between the meridional displacement of the ITCZ-SPSH system and the regional fluvial and aeolian terrigenous input variability. The ITCZ-SPSH system northern displacement during the second period of the MCA and the CWP was associated with the intensification of the Walker cell and La Niña Like conditions, resulting in stronger winds, upwelling-favorable conditions, enhanced marine productivity and greater

oxygen depletion in the water column. In contrast, the southward migrations of the ITCZ-SPSH system during the LIA correspond to an enhancement to the South American Monsoon circulation and El Niño like conditions, driving the increase in the precipitation and the terrigenous fluvial input to the Pisco continental shelf, lower productivity and increased oxygenation. Two patterns observed during the MCA, respectively marked by fluvial intensification and wind intensification, could have been forced by Pacific Ocean variability at multidecadal timescales. Further studies of the paleo-wind reconstruction at high time-resolution, combined with model simulation, are needed to better understand the interplay between the Pacific and Atlantic Ocean connection on climate variability as evidenced by McGregor et al., (2014) in the modern Pacific climate pattern.

## 5. Acknowledgements

This work was supported by the International Joint Laboratory "PALEOTRACES" (IRD-France, UPMC-France, UFF-Brazil, UA-Chile, UPCH-Peru), the Department of Geochemistry of the Universidade Federal Fluminense-UFF (Brazil), the ALYSES analytical platform (IRD/UPMC, supported by grants from Région Ile-de-France), the Peruvian Marine Research Institute (IMARPE) and the Geophysical Peruvian Institute (IGP). It was also supported by the collaborative project Chaire Croisée PROSUR (IRD). We deeply thank the CAPES-Brazil for the scholarship to Francisco Briceño Zuluaga. We give special thanks to Dr. Ioanna Bouloubassi and Dr. Phil Meyers by their comments and suggestions. We are also grateful to the anonymous reviewers for their constructive and helpful suggestions to improve this manuscript.

## 7. Bibliography

- An, F., Ma, H., Wei, H. and Lai, Z.: Distinguishing aeolian signature from lacustrine sediments of the Qaidam Basin in northeastern Qinghai-Tibetan Plateau and its palaeoclimatic implications, *Aeolian Res.*, 4, 17–30, doi:10.1016/j.aeolia.2011.12.004, 2012.
- Apaéstegui, J., Cruz, F. W., Sifeddine, A., Vuille, M., Espinoza, J. C., Guyot, J. L., Khodri, M., Strikis, N. and Perú, G.: Hydroclimate variability of the northwestern Amazon Basin near the Andean foothills of Peru related to the South American Monsoon System during the last 1600 years, *Clim. Past*, 10(1), 1967–1981, doi:10.5194/cp-10-1967-2014, 2014.
- Bakun, a: Global climate change and intensification of coastal ocean upwelling., *Science*, 247(4939), 198–201, doi:10.1126/science.247.4939.198, 1990.
- Bekaddour, T., Schlunegger, F., Vogel, H., Delunel, R., Norton, K. P., Akçar, N. and Kubik, P.: Paleo erosion rates and climate shifts recorded by Quaternary cut-and-fill sequences in the Pisco valley, central Peru, *Earth Planet. Sci. Lett.*, 390, 103–115, doi:10.1016/j.epsl.2013.12.048, 2014.
- Bendix, A., Bendix, J., Gämmerler, S., Reudenbach, C. and Weise, S.: The El Niño 1997 / 98 as seen from space - rainfall retrieval and investigation of rainfall dynamics with Goes-8 and TRMM Data, in *The 2002 EUMETSAT Meteor. Satellite Conf.*, Dublin, Ireland 02-06 Sept. 2002, EUM P 36, pp. 647–652., 2002.
- Bird, B. W., Abbott, M. B., Vuille, M., Rodbell, D. T., Stansell, N. D. and Rosenmeier, M. F.: A 2,300-year-long annually resolved record of the South American summer monsoon from the Peruvian Andes., *Proc. Natl. Acad. Sci. U. S. A.*, 108(21), 8583–8,

doi:10.1073/pnas.1003719108, 2011.

Bloemsma, M. R., Zabel, M., Stuut, J. B. W., Tjallingii, R., Collins, J. a. and Weltje, G. J.: Modelling the joint variability of grain size and chemical composition in sediments, *Sediment. Geol.*, 280, 135–148, doi:10.1016/j.sedgeo.2012.04.009, 2012.

Böning, P. and Brumsack, H.: Geochemistry of Peruvian near-surface sediments, *Geochim. Cosmochim. Acta*, 68(21), 4429–4451, doi:10.1016/j.gca.2004.04.027, 2004.

Brodie, I. and Kemp, A. E. S.: Variation in Biogenic and Detrital Fluxes and Formation of Laminae in Late Quaternary Sediments from the Peruvian Coastal Upwelling Zone, *Mar. Geol.*, 116(3-4), 385–398, doi:10.1016/0025-3227(94)90053-1, 1994.

Chaigneau, A., Dominguez, N., Eldin, G., Vasquez, L., Flores, R., Grados, C. and Echevin, V.: Near-coastal circulation in the Northern Humboldt Current System from shipboard ADCP data, *J. Geophys. Res. Ocean.*, 118(10), 5251–5266, doi:10.1002/jgrc.20328, 2013.

Clement, A. C., Seager, R., Cane, M. a. and Zebiak, S. E.: An ocean dynamical thermostat, *J. Clim.*, 9(9), 2190–2196, doi:10.1175/1520-0442(1996)009<2190:AODT>2.0.CO;2, 1996.

Ehlert, C., Grasse, P., Gutiérrez, D., Salvatelli, R. and Frank, M.: Nutrient utilisation and weathering inputs in the Peruvian upwelling region since the Little Ice Age, *Clim. Past*, 11, 187–202, doi:10.5194/cpd-10-3357-2014, 2015.

England, M. H., McGregor, S., Spence, P., Meehl, G. a., Timmermann, A., Cai, W., Gupta, A. Sen, McPhaden, M. J., Purich, A. and Santoso, A.: Recent intensification of wind-driven circulation in the Pacific and the ongoing warming hiatus, *Nat. Clim. Chang.*, 4(3), 222–227, doi:10.1038/nclimate2106, 2014.

Escobar Baccaro, D. F.: Evaluacion climatologica y sinoptica del fenómeno de vientos Paracas, Universidad Nacional Agraria La Molina, Lima-Peru., 1993.

Flores-Aqueveque, V., Alfaro, S. C., Caquineau, S., Foret, G., Vargas, G. and Rutllant, J. a.: Inter-annual variability of southerly winds in a coastal area of the Atacama Desert: implications for the export of aeolian sediments to the adjacent marine environment, *Sedimentology*, 59(3), 990–1000, doi:10.1111/j.1365-3091.2011.01288.x, 2012.

Flores-Aqueveque, V., Alfaro, S., Vargas, G., Rutllant, J. a. and Caquineau, S.: Aeolian particles in marine cores as a tool for quantitative high-resolution reconstruction of upwelling favorable winds along coastal Atacama Desert, Northern Chile, *Prog. Oceanogr.*, 134, 244–255, doi:10.1016/j.pocean.2015.02.003, 2015.

Garreaud, R. D. and Falvey, M.: The coastal winds off western subtropical South America in future climate scenarios, *Int. J. Climatol.*, 29(4), 543–554, doi:10.1002/joc.1716, 2009.

Gay, S. P.: Blowing sand and surface winds in the Pisco to Chala Area, Southern Peru, *J. Arid Environ.*, 61(1), 101–117, doi:10.1016/j.jaridenv.2004.07.012, 2005.

Gomes, L., Bergametti, G., Dulac, F. and Ezat, U.: Assessing the actual size distribution of atmospheric aerosols collected with a cascade impactor, *J. Aerosol Sci.*, 21(1), 47–59, doi:10.1016/0021-8502(90)90022-P, 1990.

Gutiérrez, D., Bouloubassi, I., Sifeddine, A., Purca, S., Goubanova, K., Graco, M., Field, D., Méjanelle, L., Velazco, F., Lorre, A., Salvatelli, R., Quispe, D., Vargas, G., Dewitte, B. and Ortlieb, L.: Coastal cooling and increased productivity in the main upwelling zone off Peru since the mid-twentieth century, *Geophys. Res. Lett.*, 38(7), 1–6, doi:10.1029/2010GL046324, 2011.

Gutiérrez, D., Sifeddine, A., Field, D., Ortlieb, L., Vargas, G., Chaves, F., Velazco, F., Ferreira, V., Tapia, P., Salvatelli, R., Boucher, H., Morales, M. C., Valdes, J., Reyss, J., Campusano, A., Boussafir, M., Mandeng-Yogo, M., Garcia, M. and Baumgartner, T.: Rapid reorganization in ocean biogeochemistry off Peru towards the end of the Little Ice Age, *Biogeosciences*, 6, 835–848, 2009.

506 Gutiérrez, D., Sifeddine, A., Reyss, J., Vargas, G., Velasco, F., Salvattecí, R., Ferreira, V., Ortlieb,  
507 L., Field, D., Baumgartner, T., Boussafir, M., Boucher, H., Valdes, J., Marinovic, L., Soler, P.  
508 and Tapia, P.: Anoxic sediments off Central Peru record interannual to multidecadal changes of  
509 climate and upwelling ecosystem during the last two centuries., *Adv. Geosci.*, 6, 119–125, 2006.

510 Haney, E. M. and Grolier, M. J.: Geologic map of major Quaternary eolian features, northern and  
511 central coastal Peru, United States Geol. Surv. Misc. Investig., I-2162, 1991.

512 Haug, G. H., Hughen, K. a, Sigman, D. M., Peterson, L. C. and Röhl, U.: Southward migration of  
513 the intertropical convergence zone through the Holocene., *Science*, 293(5533), 1304–8,  
514 doi:10.1126/science.1059725, 2001.

515 Hesse, P. P. and McTainsh, G. H.: Last Glacial Maximum to Early Holocene Wind Strength in  
516 the Mid-latitudes of the Southern Hemisphere from Aeolian Dust in the Tasman Sea, *Quat. Res.*,  
517 52(3), 343–349, doi:10.1006/qres.1999.2084, 1999.

518 Hill, E. A., Hickey, B. M., Shillington, F. A., Strub, P. T., Brink, K. H., Barton, E. D. and Thomas,  
519 A. C.: Eastern Ocean Boundaries coastal segment (E), in *The Sea*, Vol 11, vol. II, edited by A.  
520 Robinson and K. Brink, pp. 29–67, John Wiley & Sons Ltd., 1998.

521 Holz, C., Stuut, J. B. W., Henrich, R. and Meggers, H.: Variability in terrigenous sedimentation  
522 processes off northwest Africa and its relation to climate changes: Inferences from grain-size  
523 distributions of a Holocene marine sediment record, *Sediment. Geol.*, 202(3), 499–508,  
524 doi:10.1016/j.sedgeo.2007.03.015, 2007.

525 Huang, X., Oberhänsli, H., von Suchodoletz, H. and Sorrel, P.: Dust deposition in the Aral Sea:  
526 implications for changes in atmospheric circulation in central Asia during the past 2000 years,  
527 *Quat. Sci. Rev.*, 30(25-26), 3661–3674, doi:10.1016/j.quascirev.2011.09.011, 2011.

528 Iversen, J. D. and White, B. R.: Saltation threshold on Earth, Mars and Venus, *Sedimentology*,  
529 29, 111–119, doi:10.1111/j.1365-3091.1982.tb01713.x, 1982.

530 Kok, J. F., Parteli, E. J. R., Michaels, T. I. and Karam, D. B.: The physics of wind-blown sand  
531 and dust, *Reports Prog. Phys.*, 75(10), 106901, doi:10.1088/0034-4885/75/10/106901, 2012.

532 Koopmann, B.: Sedimentation von Saharastaub im subtropischen Nordatlantik während der  
533 letzten 25.000 Jahre, *Meteor. Forsch. ergeb. R. C*, 35, 23–59, 1981.

534 Lavado Casimiro, W., Ronchail, J., Labat, D., Espinoza, J. C. and Guyot, J. L.: Basin-scale  
535 analysis of rainfall and runoff in Peru (1969–2004): Pacific, Titicaca and Amazonas drainages,  
536 *Hydrol. Sci. J.*, 57(4), 625–642, doi:10.1080/02626667.2012.672985, 2012.

537 Lavado-Casimiro, W. and Espinoza, J. C.: Impacts of El Nino and La Nina in the precipitation  
538 over Peru (1965-2007), *Rev. Bras. Meteorol.*, 29(2), 171–182, doi:10.1590/S0102-  
539 77862014000200003, 2014.

540 Marticorena, B.: Dust Production Mechanisms, in *Mineral Dust: A Key Player in the Earth*  
541 *System*, edited by P. Knippertz and J.-B. Stuut, pp. 93–120, Springer, Dordrecht Heidelberg New  
542 York London., 2014.

543 Marticorena, B. and Bergametti, G.: Modeling the atmospheric dust cycle: 1. Design of a soil-  
544 derived dust emission scheme, *J. Geophys. Res.*, 100(D8), 16415, doi:10.1029/95JD00690, 1995.

545 McCave, I. N., Manighetti, B. and Robinson, S. G.: Sortable silt and fine sediment  
546 size/composition slicing: parameters for palaeocurrent speed and palaeoceanography,  
547 *Paleoceanography*, 10(3), 593–610, doi:10.1029/94PA03039, 1995.

548 McGregor, S., Timmermann, A., Stuecker, M. F., England, M. H. and Merrifield, M.: Recent  
549 Walker circulation strengthening and Pacific cooling amplified by Atlantic warming, *Nat. Clim.*  
550 *Chang.*, (August), 1–5, doi:10.1038/NCLIMATE2330, 2014.

551 McPhillips, D., Bierman, P. R., Crocker, T. and Rood, D. H.: Landscape response to Pleistocene-

552 Holocene precipitation change in the Western Cordillera, Peru: 10 Be concentrations in modern  
553 sediments and terrace fills, *J. Geophys. Res. Earth Surf.*, 118(4), 2488–2499,  
554 doi:10.1002/2013JF002837, 2013.

555 McTainsh, G. H., Nickling, W. G. and Lynch, a. W.: Dust deposition and particle size in Mali,  
556 West Africa, *Catena*, 29(3-4), 307–322, doi:10.1016/S0341-8162(96)00075-6, 1997.

557 Meyer, I., Davies, G. R. and Stuut, J. B. W.: Grain size control on Sr-Nd isotope provenance  
558 studies and impact on paleoclimate reconstructions: An example from deep-sea sediments  
559 offshore NW Africa, *Geochemistry, Geophys. Geosystems*, 12(3), 14,  
560 doi:10.1029/2010GC003355, 2011.

561 Molina-Cruz, A.: The relation of the southern trade winds to upwelling processes during the last  
562 75,000 years, *Quat. Res.*, 8(3), 324–338, doi:10.1016/0033-5894(77)90075-8, 1977.

563 Montes, I., Colas, F., Capet, X. and Schneider, W.: On the pathways of the equatorial subsurface  
564 currents in the eastern equatorial Pacific and their contributions to the Peru-Chile Undercurrent,  
565 *J. Geophys. Res. Ocean.*, 115(9), 1–16, doi:10.1029/2009JC005710, 2010.

566 Morera, S., Condom, T., Crave, A. and Galvez, C.: Tasas de erosión y dinámica de los flujos de  
567 sedimentos en la cuenca del río Santa , Perú, *Rev. Peru. Geo-Atmosférica RPGA*, 37(3), 25–37,  
568 2011.

569 Oppo, D. W., Rosenthal, Y. and Linsley, B. K.: 2,000-year-long temperature and hydrology  
570 reconstructions from the Indo-Pacific warm pool., *Nature*, 460(7259), 1113–1116,  
571 doi:10.1038/nature08233, 2009.

572 Ortlieb, L.: The Documented Historical Record of El Nino Events in Peru: An Update of the  
573 Quinn Record (Sixteenth through Nineteenth Centuries), in *El Nino and the Southern Oscillation*,  
574 *Multiscale Variability and Global and Regional Impacts*, pp. 207–295., 2000.

575 Parkin, D. W. and Shackleton, N. .: Trade wind and temperature correlations down a deep sea  
576 core off the Sharan coast, *Nature*, 245, 455–457, 1973.

577 Peterson, L. and Haug, G.: Variability in the mean latitude of the Atlantic Intertropical  
578 Convergence Zone as recorded by riverine input of sediments to the Cariaco Basin (Venezuela),  
579 *Palaeogeogr. Palaeoclimatol. Paleooceanogr.*, 234, 97–113, doi:10.1016/j.palaeo.2005.10.021,  
580 2006.

581 Pichevin, L., Cremer, M., Giraudeau, J. and Bertrand, P.: A 190 ky record of lithogenic grain-size  
582 on the Namibian slope: Forging a tight link between past wind-strength and coastal upwelling  
583 dynamics, *Mar. Geol.*, 218(1-4), 81–96, doi:10.1016/j.margeo.2005.04.003, 2005.

584 Prins, M.: Pelagic, hemipelagic and turbidite deposition in the Arabian Sea during the late  
585 Quaternary: Unravelling the signals of aeolian and fluvial sediment supply as functions of  
586 tectonics, sea-level and climate change by means of end-member modelling of silicic, Utrecht,  
587 Universiteit Utrecht., 1999.

588 Prins, M. a., Vriend, M., Nugteren, G., Vandenberghe, J., Lu, H., Zheng, H. and Jan Weltje, G.:  
589 Late Quaternary aeolian dust input variability on the Chinese Loess Plateau: inferences from  
590 unmixing of loess grain-size records, *Quat. Sci. Rev.*, 26(1-2), 230–242,  
591 doi:10.1016/j.quascirev.2006.07.002, 2007.

592 Quijano Vargas, J. J.: Estudio numerico y observacional de la dinámica de Viento Paracas,  
593 asociado al transporte eólico hacia el océano frente a la costa de Ica-Perú., Universidad Peruana  
594 Cayetano Heredia, Lima - Perú., 2013.

595 Ratmeyer, V., Fischer, G. and Wefer, G.: Lithogenic particle fluxes and grain size distributions  
596 in the deep ocean off northwest Africa: Implications for seasonal changes of aeolian dust input  
597 and downward transport, *Deep Sea Res. Part I Oceanogr. Res. Pap.*, 46, 1289–1337, 1999.

598 Rein, B.: El Niño variability off Peru during the last 20,000 years, *Paleoceanography*, 20(4),



599 PA4003, doi:10.1029/2004PA001099, 2005.

600 Rein, B.: How do the 1982/83 and 1997/98 El Niños rank in a geological record from Peru?, *Quat.*  
601 *Int.*, 161(1), 56–66, doi:10.1016/j.quaint.2006.10.023, 2007.

602 Rein, B., Lückge, A. and Sirocko, F.: A major Holocene ENSO anomaly during the Medieval  
603 period, *Geophys. Res. Lett.*, 31(17), L17211, doi:10.1029/2004GL020161, 2004.

604 Reinhardt, L., Kudrass, H., Lückge, A., Wiedicke, M., Wunderlich, J. and Wendt, G.: High-  
605 resolution sediment echosounding off Peru Late Quaternary depositional sequences and  
606 sedimentary structures of a current-dominated shelf, *Mar. Geophys. Res.*, 23(1980), 335–351,  
607 2002.

608 Reuter, J., Stott, L., Khider, D., Sinha, A., Cheng, H. and Edwards, R. L.: A new perspective on  
609 the hydroclimate variability in northern South America during the Little Ice Age, *Geophys. Res.*  
610 *Lett.*, 36(21), L21706, doi:10.1029/2009GL041051, 2009.

611 Rustic, G. T., Marchitto, T. M. and Linsley, B. K.: Dynamical excitation of the tropical Pacific  
612 Ocean and ENSO variability by Little Ice Age cooling, *Science* (80-. ), 350(6267), 1537–1541,  
613 2015.

614 Salvattecí, R., Field, D. B., Baumgartner, T., Ferreira, V. and Gutierrez, D.: Evaluating fish scale  
615 preservation in sediment records from the oxygen minimum zone off Peru, *Paleobiology*, 38(1),  
616 52–78, doi:10.1666/10045.1, 2012.

617 Salvattecí, R., Field, D., Sifeddine, A., Ortlieb, L., Ferreira, V., Baumgartner, T., Caqueneau, S.,  
618 Velasco, F., Reyss, J. L., Sanchez-Cabeza, J. A. and Gutierrez, D.: Cross-stratigraphies from a  
619 seismically active mud lens off Peru indicate horizontal extensions of laminae, missing sequences,  
620 and a need for multiple cores for high resolution records, *Mar. Geol.*, 357, 72–89,  
621 doi:10.1016/j.margeo.2014.07.008, 2014a.

622 Salvattecí, R., Gutierrez, D., Field, D., Sifeddine, A., Ortlieb, L., Bouloubassi, I., Boussafir, M.,  
623 Boucher, H. and Cetin, F.: The response of the Peruvian Upwelling Ecosystem to centennial-scale  
624 global change during the last two millennia, *Clim. Past*, 10(1), 1–17, doi:10.5194/cp-10-1-2014,  
625 2014b.

626 Salvattecí, R., Gutierrez, D., Sifeddine, A., Ortlieb, L., Druffel, E., Boussafir, M. and Schneider,  
627 R.: Centennial to millennial-scale changes in oxygenation and productivity in the Eastern Tropical  
628 South Pacific during the last 25,000 years, *Quat. Sci. Rev.*, 131, 102–117,  
629 doi:10.1016/j.quascirev.2015.10.044, 2016.

630 Saukel, C., Lamy, F., Stuut, J. B. W., Tiedemann, R. and Vogt, C.: Distribution and provenance  
631 of wind-blown SE Pacific surface sediments, *Mar. Geol.*, 280(1-4), 130–142,  
632 doi:10.1016/j.margeo.2010.12.006, 2011.

633 Scheidegger, K. F. and Krissek, L. A.: Dispersal and deposition of eolian and fluvial sediments  
634 off Peru and northern Chile., *Geol. Soc. Am. Bull.*, 93(2), 150–162, doi:10.1130/0016-  
635 7606(1982)93<150:DADOEA>2.0.CO;2, 1982.

636 Schweigger, E.: *El litoral peruano (Segunda edición)*., Lima: Universidad Nacional “Federico  
637 Villarreal”, 1964., 1984.

638 Sears, M.: Notes on the Peruvian coastal current. 1. An introduction to the ecology of Pisco Bay,  
639 *Deep Sea Res.*, 1(3), 141–169, doi:10.1016/0146-6313(54)90045-3, 1954.

640 Shao, Y., Ishizuka, M., Mikami, M. and Leys, J. F.: Parameterization of size-resolved dust  
641 emission and validation with measurements, *J. Geophys. Res. Atmos.*, 116(January), 1–19,  
642 doi:10.1029/2010JD014527, 2011.

643 Shao, Y. and Lu, H.: A simple expression for wind erosion threshold friction velocity, *J. Geophys.*  
644 *Res.*, 105(d), 22437, doi:10.1029/2000JD900304, 2000.

645 Sifeddine, A., Gutiérrez, D., Ortlieb, L., Boucher, H., Velazco, F., Field, D., Vargas, G.,  
646 Boussafir, M., Salvatelli, R., Ferreira, V., García, M., Valdés, J., Caquineau, S., Mandeng Yogo,  
647 M., Cetin, F., Solis, J., Soler, P. and Baumgartner, T.: Laminated sediments from the central  
648 Peruvian continental slope: A 500 year record of upwelling system productivity, terrestrial runoff  
649 and redox conditions, *Prog. Oceanogr.*, 79(2-4), 190–197, doi:10.1016/j.pocean.2008.10.024,  
650 2008.

651 Smith, R. L.: Circulation patterns in upwelling regimes, *Coast. upwelling*, 13–35, 1983.

652 Strub, P. T., Mesías, J. M. J. M., Montecino, V., Rutllant, J. A., Salinas, S., Robinson, A. R. and  
653 Brink, K. H.: Coastal ocean circulation off western South America, in *The Sea*, vol. 11, pp. 273–  
654 313., 1998.

655 Stuut, J. W., Prins, M. A. and Weltje, G. J.: The palaeoclimatic record provided by aeolian dust  
656 in the deep sea: proxies and problems, *Geophys. Res. Abstr.*, 7, 10886, doi:1607-  
657 7962/gra/EGU05-A-10886, 2005.

658 Stuut, J.-B. W., Kasten, S., Lamy, F. and Hebbeln, D.: Sources and modes of terrigenous sediment  
659 input to the Chilean continental slope, *Quat. Int.*, 161(1), 67–76,  
660 doi:10.1016/j.quaint.2006.10.041, 2007.

661 Stuut, J.-B. W. and Lamy, F.: Climate variability at the southern boundaries of the Namib  
662 (southwestern Africa) and Atacama (northern Chile) coastal deserts during the last 120,000 yr,  
663 *Quat. Res.*, 62(3), 301–309, doi:10.1016/j.yqres.2004.08.001, 2004.

664 Stuut, J.-B. W., Prins, M. a., Schneider, R. R., Weltje, G. J., Jansen, J. H. F. and Postma, G.: A  
665 300-kyr record of aridity and wind strength in southwestern Africa: inferences from grain-size  
666 distributions of sediments on Walvis Ridge, SE Atlantic, *Mar. Geol.*, 180(1-4), 221–233,  
667 doi:10.1016/S0025-3227(01)00215-8, 2002.

668 Suess, E., Kulm, L. D. and Killingley, J. S.: Coastal upwelling and a history of organic-rich  
669 mudstone deposition off Peru, *Geol. Soc. London, Spec. Publ.*, 26(1), 181–197,  
670 doi:10.1144/GSL.SP.1987.026.01.11, 1987.

671 Sun, D., Bloemendal, J., Rea, D. ., Vandenberghe, J., Jiang, F., An, Z. and Su, R.: Grain-size  
672 distribution function of polymodal sediments in hydraulic and aeolian environments, and  
673 numerical partitioning of the sedimentary components, *Sediment. Geol.*, 152(3-4), 263–277,  
674 doi:10.1016/S0037-0738(02)00082-9, 2002.

675 Sydeman, W. J., García-Reyes, M., Schoeman, D. S., Rykaczewski, R. R., Thompson, S. a, Black,  
676 B. a and Bograd, S. J.: Climate change and wind intensification in coastal upwelling ecosystems.,  
677 *Science*, 345(6192), 77–80, doi:10.1126/science.1251635, 2014.

678 Timmermann, A., Okumura, Y., An, S. I., Clement, a., Dong, B., Guilyardi, E., Hu, a., Jungclaus,  
679 J. H., Renold, M., Stocker, T. F., Stouffer, R. J., Sutton, R., Xie, S. P. and Yin, J.: The influence  
680 of a weakening of the Atlantic meridional overturning circulation on ENSO, *J. Clim.*, 20(19),  
681 4899–4919, doi:10.1175/JCLI4283.1, 2007.

682 Unkel, I., Kadereit, A., Mächtle, B., Eitel, B., Kromer, B., Wagner, G. and Wacker, L.: Dating  
683 methods and geomorphic evidence of palaeoenvironmental changes at the eastern margin of the  
684 South Peruvian coastal desert (14°30'S) before and during the Little Ice Age, *Quat. Int.*, 175(1),  
685 3–28, doi:10.1016/j.quaint.2007.03.006, 2007.

686 Weltje, G. J.: End-member modeling of compositional data: Numerical-statistical algorithms for  
687 solving the explicit mixing problem, *Math. Geol.*, 29(4), 503–549, doi:10.1007/BF02775085,  
688 1997.

689 Weltje, G. J. and Prins, M. a: Muddled or mixed? Inferring palaeoclimate from size distributions  
690 of deep-sea clastics, *Sediment. Geol.*, 162(1-2), 39–62, doi:10.1016/S0037-0738(03)00235-5,  
691 2003.

692     Weltje, G. J. and Prins, M. a.: Genetically meaningful decomposition of grain-size distributions,  
693     Sediment. Geol., 202(3), 409–424, doi:10.1016/j.sedgeo.2007.03.007, 2007.

694     Wentworth, C. K.: A Scale of Grade and Class Terms for Clastic Sediments, J. Geol., 30(5), 377–  
695     392, doi:10.1086/622910, 1922.

696

697 Table 1: Averaged parameters (geometric mean diameter (Gmd), amplitude (A) and geometric standard deviation (Gsd)) of the 4 log-normal modes (components)  
698 identified from measured size distributions of sediment samples (B6 and G10 cores).

699

700

701

M1			M2			M3			M4		
Gmd ( $\mu\text{m}$ )	A (%)	Gsd	Gmd ( $\mu\text{m}$ )	A (%)	Gsd	Gmd ( $\mu\text{m}$ )	A (%)	Gsd	Gmd ( $\mu\text{m}$ )	A (%)	Gsd
$3 \pm 1$	$16 \pm 7$	$1.9 \pm 0.2$	$10 \pm 2$	$43 \pm 15$	$1.9 \pm 0.2$	$54 \pm 12$	$20 \pm 10$	$1.4 \pm 0.2$	$90 \pm 13$	$20 \pm 13$	$1.2 \pm 0.2$

702

703

704

705

706

707

708

709

710

711

712

713 Table 2. Minimum, maximum and average values of the grain size components in each climate unit obtained along the record in the Pisco continental shelf.

714

715

716

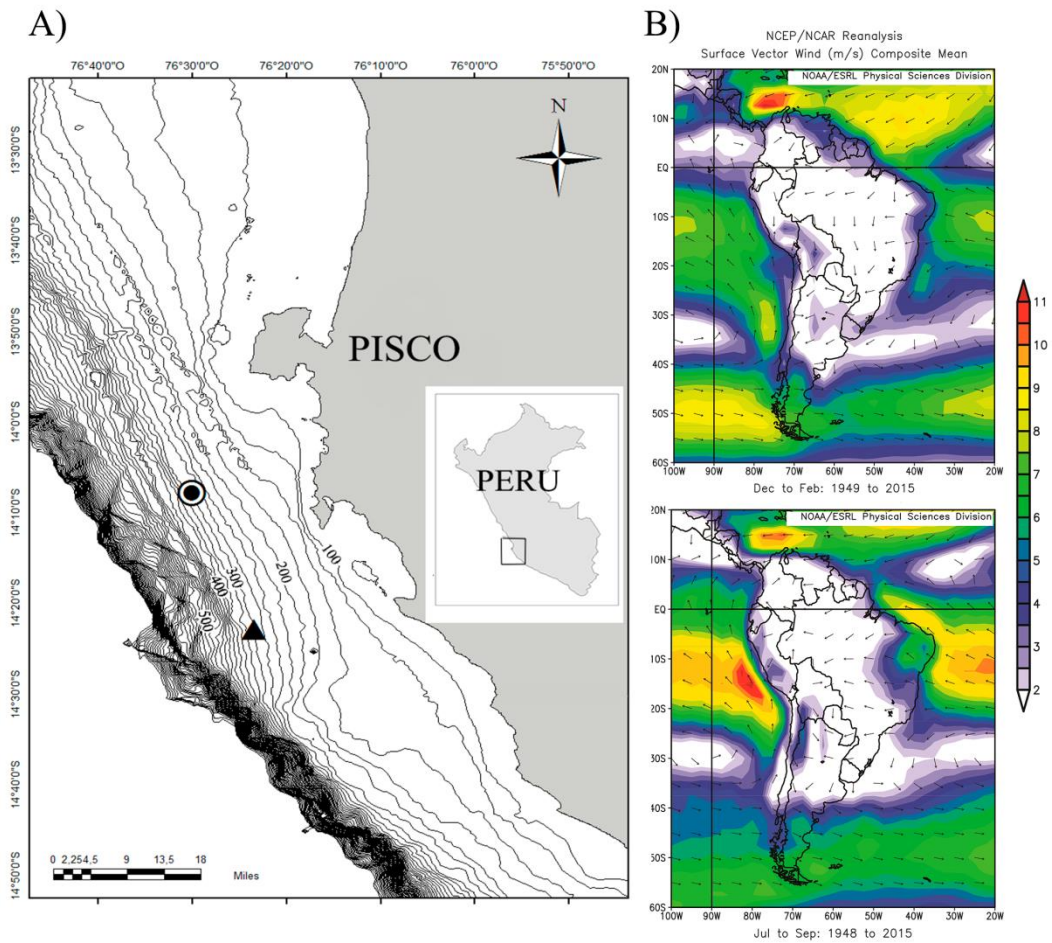
717

718

719

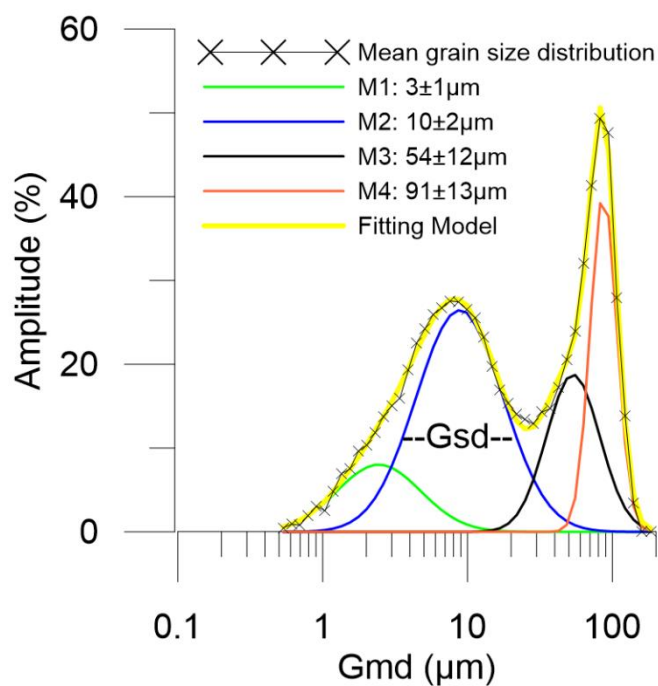
720

	First period MCA		Second period MCA		LIA		CWP	
	1050 – 1170 A.D.		1170 – 1450A.D.		1450 – 1800 A.D.		1900 A.D to present	
Grain size components	Amplitude (%)		Amplitude (%)		Amplitude (%)		Amplitude (%)	
	Av/Std.Dv.	Range (Min.-Max.)	Av/Std.Dv	Range (Min.-Max.)	Av/Std.Dv.	Range (Min.-Max.)	Av/Std.Dv.	Range (Min.-Max.)
M1	13 ± 5	8 - 19	14 ± 6	5 - 27	15 ± 6	6 - 29	18 ± 7	4 - 40
M2	50 ± 14	33 - 64	36 ± 8	23 - 60	53 ± 15	16 - 80	34 ± 10	13 - 63
M3	16 ± 8	6 - 28	21 ± 10	0 - 39	19 ± 9	4 - 45	23 ± 10	6 - 44
M4	21 ± 5	12 - 30	29 ± 15	10 - 55	14 ± 11	0 - 44	25 ± 13	0 - 56



721

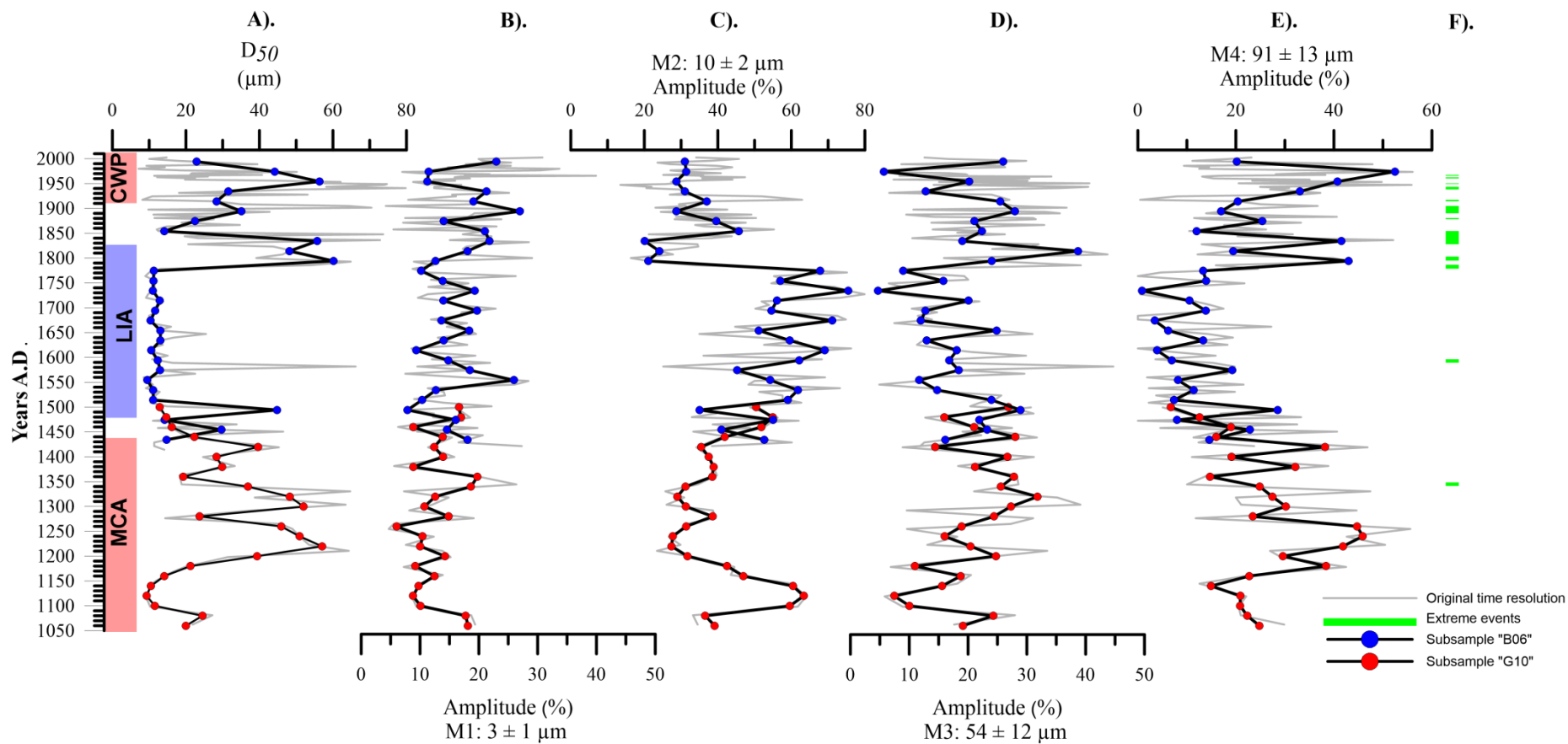
722 Figure 1. A) Location of the sampling of the sediment cores B040506 (black circle) and  
 723 G10-GC-01 (black triangle) in the Central Peru continental margin. Bathymetric contour  
 724 lines are in 25m intervals from 100m to 500 m depth. B) Mean surface vector wind  
 725 velocity (m/s) composite mean for summer (up) and winter (down) between 1948 and  
 726 2015 at South American. NCEP/NCAR Reanalysis data.



728

729 Figure 2: Comparison between a measured grain size distribution and the fitted curve using log-  
 730 normal function and its partitioning into four individual grain size modes. The measured data is  
 731 a mean grain-size distribution from all samples of B6 and G10 cores.

732 .



733

734 Figure 3. A) Median grain size (D50) variation along the record and variation in relative abundance of the sedimentary components: B) M1, C) Fluvial (M2),  
 735 D) Aeolian (M3) and E) Aeolian (M4) of the grain size distribution in the record. F) Represent the samples where was found very large particles related to  
 736 extreme events.



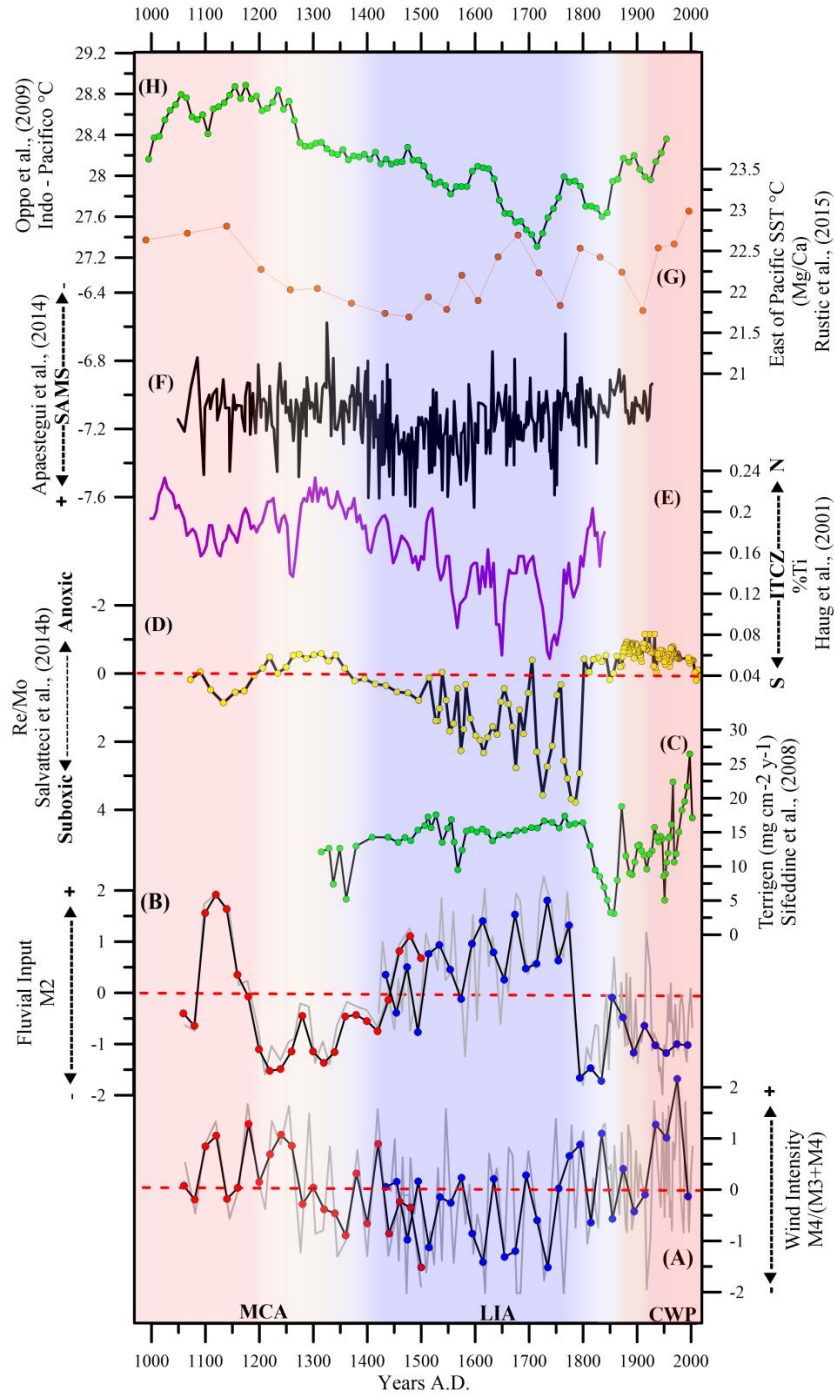


Figure 4. A) Wind intensity ( $M4/(M3+M4)$ ) anomaly reconstruction, B) Fluvial input ( $M2$ ) anomaly reconstruction on the continental shelf, and records of C) Terrigenous flux (total minerals) in Pisco continental shelf by Sifeddine et al (2008), D) OMZ activity (Re/Mo anomalies) negative values indicate more anoxic conditions (the axis was reversed) (Salvatteci et al., 2014b), E) ITCZ migration (%Ti) (Peterson and Haug, 2006), F) SAMS activity reconstruction ( $\delta^{18}\text{O}$  Palestina Cave) (Apaéstegui et al., 2014), G) Eastern temperatures reconstruction (Rustic et al., 2015) H) Indo-Pacific temperatures reconstruction (Oppo et al., 2009).